The characteristics of a Linear Joule Engine Generator operating on a dry friction principle

Ngwaka, Ugochukwu; Jia, Boru; Lawrence, Christopher; Wu, D.; Smallbone, Andrew; Roskilly, Anthony Paul

DOI:
10.1016/j.apenergy.2018.12.081

Applied Energy 237 (2019) 49–59

Contents lists available at ScienceDirect

Applied Energy

journal homepage: www.elsevier.com/locate/apenergy

The characteristics of a Linear Joule Engine Generator operating on a dry friction principle

Ugochukwu Ngwaka[a], Boru Jia[a], Christopher Lawrence[a], Dawei Wu[b], Andrew Smallbone[a,*], Anthony Paul Roskilly[a]

[a] Sir Joseph Swan Centre for Energy Research, School of Engineering, Newcastle University, Newcastle upon Tyne NE1 7RU, UK
[b] School of Engineering, Newcastle University, Newcastle upon Tyne NE1 7RU, UK

HIGHLIGHTS

- A new friction force model for a novel Linear Joule Engine Generator (LJEG) prototype is presented.
- Existing numerical friction force models are compared with experimental results.
- The relationship between friction and the LJEG dynamics are shown.

ARTICLE INFO

Keywords:
Linear-Joule Engine Generator
Friction
Electric generator

ABSTRACT

In this paper, the friction characteristics of a novel Linear Joule Engine Generator operating on dry friction mechanism is presented. A numerical model of the friction forces is represented through the development of a dry friction force model integrated into a mass-spring-damper system with viscous damping and spring constant to emulate compressor and expander operating pressures. Experimental results from a Linear Joule Engine Generator prototype are compared with the numerical simulation results predicted by the proposed friction model and other reported friction models identified from the wider engineering literature. Finally, the relationship between electric generator load and friction power of Linear Joule Engine Generator is established.

1. Introduction

The Linear-Joule Engine Generator (LJEG) combines the principles of Reciprocating Joule Cycle Engines (RJE) and Free-Piston Linear Electric Generators (FPLEG). The concept of LJEG was first proposed by the authors' group [1] and a parametric design, system analysis, and optimisation were presented [2] with a working prototype now in operation [3]. The external combustion process makes the solution compatible for a wide range of fuel applications and more adaptable to different combustion modes that could reduce nitrous oxides (NO_x) and particulate matter emissions. The linear configuration of LJEG, when compared to the conventional expansion machines, presents substantial benefits, which include high efficiency, good operational flexibility, compact in size and simple mechanical structure, low frictional losses, and improved system power to weight ratio [4].

There has been growing research interest on reciprocating Joule cycle engines for combined heat and power (CHP) and microscale electric power generation applications. Bell and Partridge [5], constructed a thermodynamic model of a reciprocating Joule cycle engine incorporating external combustor, with traditional crankshaft mechanism. The model maximum design temperature of 1300 °C. It was concluded that improved thermal efficiency could be achieved by minimizing sealing requirements to ensure less friction. It was also suggested that low friction could be achieved by utilising a relatively low-pressure ratio. The model predicted a thermal efficiency of 50% for at 7.0 pressure ratio, without considering thermal losses. Researchers from the authors' group [6] considered a reciprocating Joule cycle engine for CHP application with crankshaft mechanism and a recuperator. The results showed that thermal efficiency is proportional to operating pressure ratio and peak temperature. An engine efficiency of 38% and electrical efficiency of 33% were achieved in the model. A similar study [7] by researchers in France explored a static model of Joule engine with an external heat source for CHP application, a peak temperature of 650 °C and a pressure ratio of 6.0 were achieved at a thermal efficiency of 37.6%. A study on a dynamic model of open Joule cycle low-speed two-stroke engine for micro co-generation systems,

* Corresponding author.
E-mail address: andrew.smallbone@ncl.ac.uk (A. Smallbone).

https://doi.org/10.1016/j.apenergy.2018.12.081
Received 3 September 2018; Received in revised form 21 December 2018; Accepted 30 December 2018
Available online 07 January 2019

Nomenclature

A_c	compressor piston area (m^2)
A_d	reference flow area (m^2)
A_e	expander piston area (m^2)
c	damping coefficient (–)
C_d	discharge coefficient (–)
$F(t)$	excitation force (N)
$\vec{F_e}$	pressure force from linear expander (N)
$\vec{F_{el}}$	pressure force from left chamber of the expander (N)
$\vec{F_{er}}$	pressure force from right chamber of the expander (N)
$\vec{F_c}$	pressure force from linear the compressor (N)
$\vec{F_{cl}}$	pressure force from left chamber the compressor (N)
$\vec{F_{cr}}$	pressure force from right chamber the compressor (N)
F_f	friction force (N)
F_{fd}	dry contact friction force (N)
F_{fl}	friction force relative to retardation phase (N)
F_{fp}	pressure friction force (N)
F_{fu}	friction force relative to acceleration phase (N)
$\vec{F_g}$	generator force (N)
F_{net}	resultant force (N)
f_s	static friction coefficient (–)
f_d	dynamic friction coefficient (–)
G	linear generator load constant ($N/(m{\cdot}s^{-1})$)
h	coefficient of heat transfer ($W/m^2{\cdot}K$)
h_e	specific enthalpy of the mass flow through the expander (J/kg)
k	spring constant (–)
m	moving mass (kg)
$\dot{m}$	mass flowrate through valves (kg/s)
$\dot{m}_c$	mass flowrate through the compressor (kg/s)
$\dot{m}_e$	mass flowrate through the expander (kg/s)
N	ring normal pressure force (N)
f	friction function (–)
P_a	atmospheric pressure (bar)
p_c	pressure in the compressor (Pa)
p_{cl}	pressure in the left compressor (Pa)
p_{cr}	pressure in the right compressor (Pa)
p_d	downstream pressure (Pa)
p_e	pressure in the expander (Pa)
p_{el}	pressure in the left expander (Pa)
p_{er}	pressure in the right expander (Pa)
p_u	upstream pressure (Pa)
$p_{i/o}$	suction or discharge compressor fluid pressure (Pa)
$\dot{Q}_h$	heat flow rate (J/s)
R	gas constant (J/kg K)
T_u	temperature of upstream (K)
T_w	average surface temperature of the cylinder wall (K)
x	piston displacement (m)
$\dot{x}$	piston sliding velocity (m/s)
$\dot{x}_m$	mean piston velocity (m/s)
$\ddot{x}$	piston acceleration $(m/s)^2$
$\ddot{x}_m$	mean piston acceleration $(m/s)^2$
V	instantaneous cylinder volume (m^3)
V_c	working volume of linear compressor (m^3)
V_e	working volume of linear expander (m^3)
a_1	friction parameters (–)
a_2	friction parameters (–)
z_1	friction parameters (–)
z_2	friction parameters (–)
$\rho_{i/o}$	suction/discharge compressor fluid density (kg/m^3)
γ	heat capacity ratio (–)

with a crankshaft mechanism, suggested that the use of a regeneration cycle for waste heat recovery can enhance the engine performances. The Joule Engine was found to be well suited for micro co-generation systems with a potential thermal efficiency of 23% at 4.0 pressure ratio [8]. Mikalsen and Roskilly [1] took a different approach by employing free piston reciprocating Joule cycle for CHP application. A double acting free piston expander and compressor, a constant pressure external combustor and recuperator were adopted. The model predicted electric conversion efficiency of 32% at 6.0 pressure ratio. Wu and Roskilly [2] conducted a parametric study on linear Joule cycle engine, an electric conversion efficiency of 32% was achieved at 800 °C and pressure ratio of 5.9. Wu, Jalal, and Baker [9] presented a coupled dynamic model of linear Joule cycle engine with embedded permanent magnet linear alternator. The coupled model also enables an integrated design of linear Joule engine and linear alternator. In this work, the maximum temperature of an external heat source was set at 790 °C and the compression ratio of the engine is 6.5, a thermal efficiency of 34% and an electric conversion efficiency of 30% was predicted. Researchers from the authors' group [3] presented a detailed dynamic and thermodynamic model of LJEG, model validation was implemented with test data from both Reciprocating Joule Engine prototype and LJEG prototype. The model predicted that electric power output can reach 4.4 kWe, while the engine thermal efficiency can reach above 34% with an electric conversion efficiency of 30%. An experimental study conducted on Free-Piston Expander Linear Generator for Organic Rankine Cycle [10] using compressed air at 1.4 bar as the working fluid, reported an indicated efficiency of 92.8% at operation frequency of 2.0 Hz. With increase expander intake pressure, the cycle to cycle variation of the Free-Piston Expander Linear Generator prototype decreases and the motion stability improves. In a similar report [11] but with a maximum intake pressure of 3.0 bar, the energy conversion efficiency of the Free-Piston Expander Linear Generator tends to increase gradually with intake pressure and external load resistance until it reaches a peak and then the energy conversion efficiency starts to decrease with the intake pressure and external load resistance. A peak value of 73.3% indicated efficiency was reported.

Friction losses are considered among the major factors that limit system performance of most mechanical systems. They affect the energy footprint of a system through wear and decrease in energy conversion efficiency. In a traditional internal combustion engine, piston assembly can be responsible for 45% of total frictional losses and most of piston assembly losses can be directly attributed to piston ring – cylinder liner interface [12]. In free piston engines, friction loss at piston ring – cylinder liner interface accounts for more than 55% of total frictional loss [13]. Friction loss in Free Piston Engine (FPE) is expected to be lower than that of traditional internal combustion engines due to the elimination of the piston skirt and crank mechanism. However, there are few research publications on friction characteristics of FPE configurations. Among the few, most of the published research articles investigated internal combustion FPEs, where hydrodynamic lubrication is predominant. In a study on the oscillation characteristic of free piston engine generator [14] considers frictional force in FPE to be a damping force, which is directly proportional to piston sliding velocity while the direction of friction is opposite to piston velocity. Similarly, the paper [15] by researchers from China described the frictional force in FPE as a damping force which can be regarded to have a linear relationship with the piston velocity. A study on Free-Piston Expander Linear Generator for small-scale Organic Rankine Cycle [16] suggested that the frictional force behaves like a viscous force that is directly proportional to piston sliding velocity. Goldsborough and Van Blarigan [17] analysed frictional force in FPE as the sum of Coulomb and viscous frictions, the viscous friction is proportional to piston velocity, where the direction of

the sum of frictional forces is opposite to piston velocity. Lee [18] used the same approach to use Coulomb and viscous friction to simulate friction force in a Free Piston Linear Generator Engine. A study on Free-Piston Expander Linear Generator without lubrication identified that Coulomb and viscous frictions are the main types of friction acting on the system, the authors applied the Coulomb and viscous friction parameters of 98.3 and 178.6 respectively for their calculation [19].

The friction force of FPE with opposed piston configuration [20] was described for a two-stroke spark ignition system to be a constant numerical value over the full stroke. Similarly, a study on a single-cylinder, two-stroke spark ignition FPE [21] proposed that the friction force is a constant numerical value over the full stroke. Meanwhile, Mikalsen and Roskilly [22] suggested that the friction force for two-stroke compression ignition FPE could be taken to be a constant numerical value all through the stroke. Yuan, Xu and He [23] claimed that friction force of FPE is affected by in-cylinder gas conditions and piston dynamics and therefore stated that friction force of FPE cannot be considered as a constant. Hence they presented a friction model that consists of three friction components: viscous friction, Coulomb friction, and friction as a result of in-cylinder pressure.

A fundamental lubrication theoretical model applicable to conventional crankshaft engines was proposed in the paper [13], which was used to simulate dynamic friction behaviour of FPEs. The results showed that friction force from piston ring – cylinder liner interface can be higher in FPEs than in crankshaft engines. Nevertheless, the elimination of crankshaft in FPEs reduces overall frictional loss, which is around half of overall frictional loss in a crankshaft engine.

Many engine developers and researchers concluded that a reduction in friction loss in engine components is a positive means in the improvement of engine's mechanical efficiency [24]. Very few detailed studies have been carried out on friction of FPEs. The most of the published studies on friction force analysis only covered opposed piston type FPEs adopting conventional lubrication principles. Although dry friction theories have been well established, it still remains a challenging task to analyse a dynamic system with dry friction components, while sources of excitation are as fluctuant as observed in LJEG applications. In order to reduce the power loss as a result of friction in an engine, an understanding is required on how engine parameters affect its friction characteristics. As such, there is a need to develop a bespoke model to represent the friction processes of LJEG; this will help to develop analytical tools for the design of low friction engine components, understand the optimal range of engine operational parameters to minimise friction loss and to develop a robust friction model that can be used in dynamic LJEG simulation to estimate actual engine-generator output. In this paper, a novel friction model for an LJEG with FPE configuration operating on dry friction principle is presented and the model is validated with respect to observed experimental data.

2. System configuration and model description

2.1. System information

Fig. 1 shows a schematic, 3D drawing and photo of the LJEG prototype. The main components are a linear compressor, a linear expander, an external reactor (combustor) and a linear generator. Two free-pistons are placed in a double acting compressor (right end) cylinder and double acting expander (left end) cylinder respectively Fig. 1(a). A rigid piston rod connects the two pistons to the linear

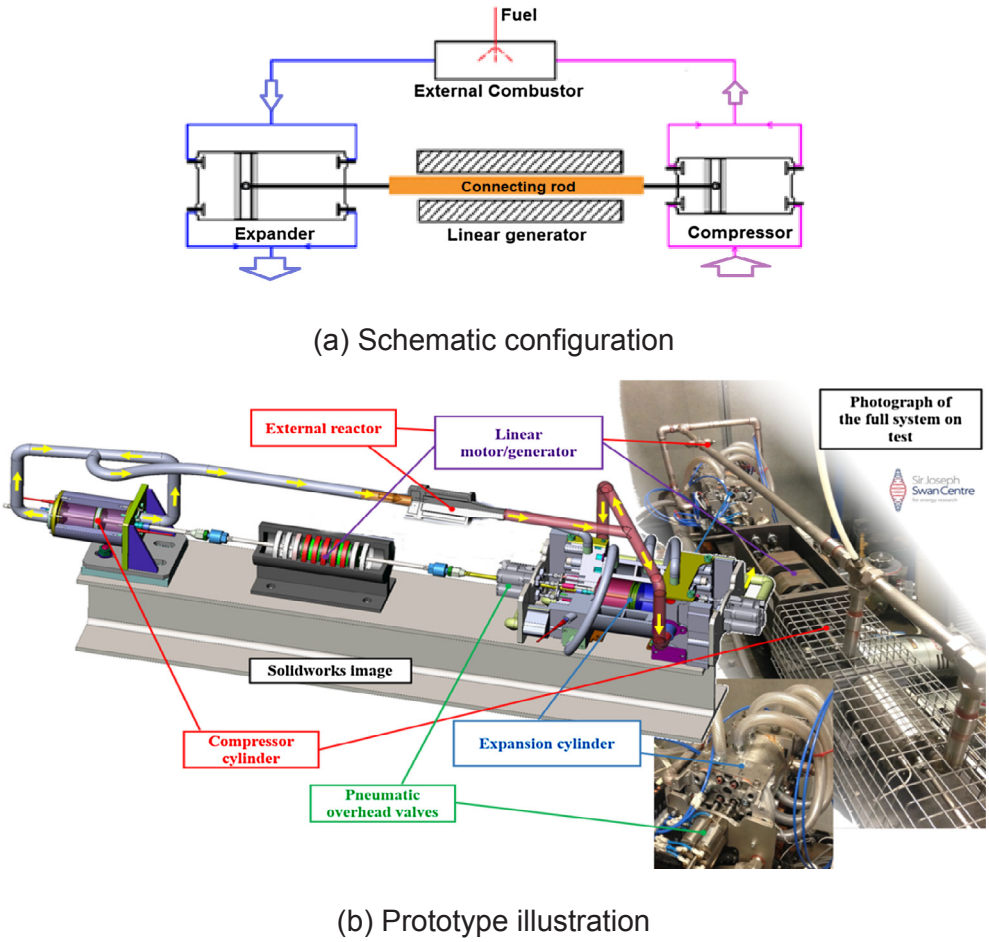

Fig. 1. Linear Joule Engine Generator prototype at Newcastle University.

alternator at the centre. Located on the compressor and the expander are the intake and exhaust valves at each end to draw in and expel working fluid. The cycle starts from the compressor where the working fluid is compressed and fed into an external combustor where the energy of the working fluid is raised to a constant pressure. The high energy fluid from the combustor is expanded in the expander of the LJEG. The expansion work drives the linear generator to produce electricity and powers the compressor to increase pressure of working fluid. More information about the system configuration can be found elsewhere [3].

2.2. LJEG dynamic structure

The piston dynamics are determined by forces acting on it, which are the gas pressure forces from the linear expander and compressor, the resistance force from the linear generator, the in-cylinder frictional force, and the inertia of the moving mass. The forces acting on the piston of LJEG as shown in Fig. 2, can be expressed as follows according to the Newton's Second Law:

$$\vec{F_e} + \vec{F_c} + \vec{F_g} + \vec{F_f} = m\ddot{x} \tag{1}$$

$$\vec{F_e} = \vec{F_{el}} + \vec{F_{er}} \tag{2}$$

$$\vec{F_c} = \vec{F_{cl}} + \vec{F_{cr}} \tag{3}$$

where $\vec{F_e}$ (N) is the pressure force from the linear expander; $\vec{F_{el}}$ (N) is the pressure force from the left chamber of the linear expander; $\vec{F_{er}}$ (N) is the pressure force from the right chamber of the linear expander; $\vec{F_c}$ (N) is the pressure force from the linear compressor; $\vec{F_{cl}}$ (N) is the pressure force from the left chamber of the linear compressor; $\vec{F_{cr}}$ (N) is the pressure force from the right chamber of the compressor. $\vec{F_f}$ (N) is the friction force, $\vec{F_g}$ (N) is the generator force, $\ddot{x}$ (m/s^2) represents piston acceleration, m (kg) is the moving mass. The gas pressure forces from both chambers of the linear expander and compressor can be obtained using the gas pressure and piston effective area.

$$\vec{F_{el}} = p_{el} \cdot A_e \tag{4}$$

$$\vec{F_{er}} = p_{er} \cdot A_e \tag{5}$$

$$\vec{F_{cl}} = p_{cl} \cdot A_c \tag{6}$$

$$\vec{F_{cr}} = p_{cr} \cdot A_c \tag{7}$$

where p_{el} (Pa) and p_{er} (Pa) are the cylinder pressure in the left and right chamber of the expander respectively. p_{cl} (Pa) and p_{cr} (Pa) are the cylinder pressure in the left chamber of the compressor respectively. A_e (m^3) and A_c (m^3) represent the piston cross-section areas of the expander and compressor respectively.

2.3. Friction model

A simple approach to model the frictional force of the LJEG is proposed. The mathematical expressions of the friction model are developed based on experimental observation and other established friction characteristics. The friction model presented has two components, the first is the static and dynamic dry contact friction of the piston ring and the cylinder liner while the second part is friction due to pressure loading. The total friction is represented by Eq. (8). The following assumptions were made for Eq. (8); the cylinder liner and the piston ring are in direct contact in the LJEG, as the piston has a crosshead piston arrangement without any side forces, piston skirt friction is neglected, the piston ring does not twist, thermal and elastic deformation of the ring and the cylinder liner are neglected, the dynamic and static friction coefficients do not vary with pressure and temperature.

$$F_f = \text{Dry contact friction force} + \text{Pressure friction loading} = F_{fd} + F_{fp} \tag{8}$$

where F_f is the total friction force, F_{fd} expresses the dry contact friction force, F_{fp} is the pressure friction force.

Eq. (1) can be simplified to a one-degree forced vibration system [25] and represented as a forced vibration system with viscous damping and spring constant [26] as illustrated in the schematic shown in Fig. 3. The system shown in Fig. 3 can be described as a model of one degree of freedom mechanical oscillator, which a dry friction damper is attached to it and its system dynamics is described by a second order differential equation as depicted in Eq. (9).

$$m\ddot{x} + c\dot{x} + kx = F(t) \tag{9}$$

$$F(t) = F_e - Nf \tag{10}$$

where c is the damping coefficient; k the spring constant, and $F(t)$ is the continuing excitation force; F_e is the force provided by expander; N is the ring normal pressure force; f is a friction function. The analogy between a mass-spring-damper and the LJEG system is expressed in Table 1.

The static and dynamic dry contact friction of the LJEG is modelled as a dry friction oscillator as represented in Fig. 3. Other assumptions included that the ring does not twist and there is no thermal and elastic deformation on the ring and the cylinder liner. Therefore only frictional force during macroscopic sliding motion with very short stops is considered rather than the stick-slip motion of the contact surface. The stick-slip effect is neglected since the piston is accelerated with a force much larger than the stiction force [19]. Dry friction problems have been investigated extensively [27]. For a dynamic system where a relative velocity between contact surfaces is virtually constant, then a simplest friction model described by the Coulomb law would serve [28]. In the LJEG and in most practical cases, the relative velocity between the contact surfaces varies hugely and changes its sign. In such conditions, the preferred model must account for the transition from static to dynamic friction and must provide a means of guiding the system through zero relative velocity [28]. A dynamic model that could account for the hysteretic behaviour of dry friction force during macroscopic sliding at variable velocity was proposed in the paper [29] and it showed that non-reversible friction characteristics depend on both relative acceleration and velocity of contact surfaces. The dry friction model adopted for our analysis is presented by [28] and represented in Eq. (11). The materials for the contact surfaces (i.e. the cylinder liner and the piston ring) are graphite on steel.

$$F_{fd} = \begin{cases} F_{fu}, sgn(\ddot{x}) > 0 F_{fu} = N f_d \left[1 + \frac{f_s - f_d}{f_d} g(\ddot{x})\right] \\ F_{fl}, sgn(\ddot{x}) < 0 F_{fl} = N f_d \left[1 - \frac{f_s - f_d}{f_d} g(\ddot{x})\right] \end{cases} \tag{11}$$

$$g(\ddot{x}) = exp\left(-\frac{a_1 |\dot{x}|}{|\ddot{x}| + a_2}\right) \tag{12}$$

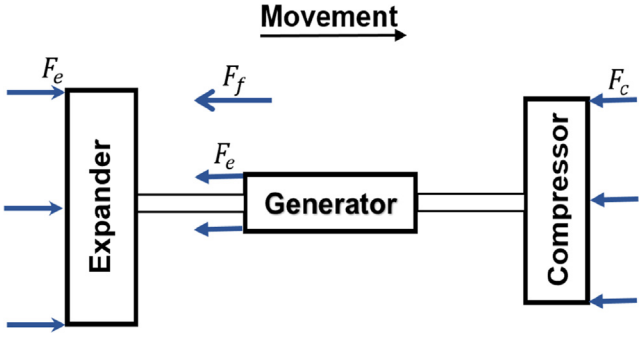

Fig. 2. Schematic of the forces acting on the piston of LJEG.

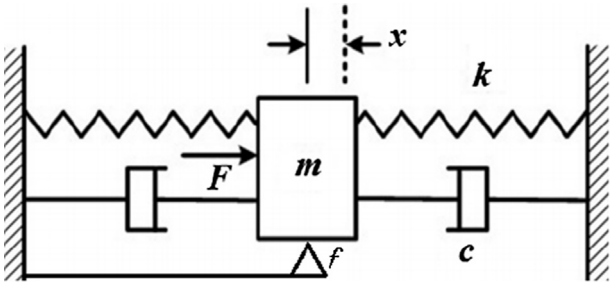

Fig. 3. Analogous forced vibration system.

Table 1
Analogy between a mass-spring damper and the LJEG system.

Mass-spring damper	LJEG system
Moving mass, m	Mass of the piston assembly
Damping coefficient, c	Linear generator load force
Spring constant, k	In-cylinder compressor force
Excitation force, $\boldsymbol{F}$	Excitation force
Normal force, N	Piston ring normal force
Friction function, f	Inter-surface friction coefficient

where a_1, a_2 (> 0) are the constant parameters, f_s, f_d are the static and dynamic friction coefficients respectively, $F_{fu,}$ and F_{fl} represent the friction forces relative to acceleration and retardation phases respectively. Eqs. (11) and (12) as well model the frictional memory during the slip phase by the function a_1 and a_2, while non-reversibility is modelled by + and − signs in quadratic brackets of Eq. (11). The frictional force due to system pressure loading is expressed as:

$$F_{fp} = \frac{bP_c}{P_a} e^{\left(\frac{b\dot{x}_m}{1+|\dot{x}|}+\frac{bP_c}{P_a}\right)} \tag{13}$$

$$b = \left(\frac{z_1}{|\ddot{x}_m| + z_2}\right) \tag{14}$$

where P_c is the pressure in the compressor cylinder (bar), P_a atmospheric pressure (bar), $|\dot{x}|$ the absolute piston sliding velocity (m/s), $\dot{x}_m$ the mean piston velocity (m/s), $\ddot{x}_m$ the mean piston acceleration (m/s^2), z_1 and z_2 are friction parameters.

2.4. LJEG dynamic and thermodynamic model

A detailed description of the dynamic and thermodynamic model of the LJEG can be found in the previous paper [3]. The in-cylinder thermodynamic relationship in the linear expander and compressor can be described by Eq. (15) [3]. Utilising the conservation of energy principle in a control volume yields Eq. (16)

$$\frac{dp_e}{dt} = \frac{\gamma - 1}{V_e}\left(-\frac{dQ_h}{dt}\right) - \frac{p\gamma}{V_e}\frac{dV_e}{dt} + \frac{\gamma - 1}{V_e}\sum_i \dot{m}_e h_e \tag{15}$$

$$\frac{dp_c}{dt} = \gamma\left(\frac{p_{i/o}}{V_c \rho_{i/o}}\dot{m}_c - \frac{\dot{x}p_c}{x}\right) \tag{16}$$

where γ is the specific heat ratio, $\dot{Q}_h$ (J/s) is the heat flow rate, $\dot{m}_e$ (kg/s) is the mass flowrate through the expander; h_e (J/kg) is the specific enthalpy of the mass flow through the expander, p_e (Pa) and V_e (m^3) represent the expander pressure and expander working volume respectively. p_c (Pa) represents the pressure in the compressor cylinder, $p_{i/o}$ (Pa) represents the suction or discharge compressor fluid pressure, $\rho_{i/o}$(kg/m^3)represents the suction or discharge compressor fluid density, $\dot{m}_c$(kg/s) suction or discharge compressor fluid mass flow rate. V_c (m^3) compressor working volume. x(m) is the piston displacement. $\dot{x}$(m/s) is

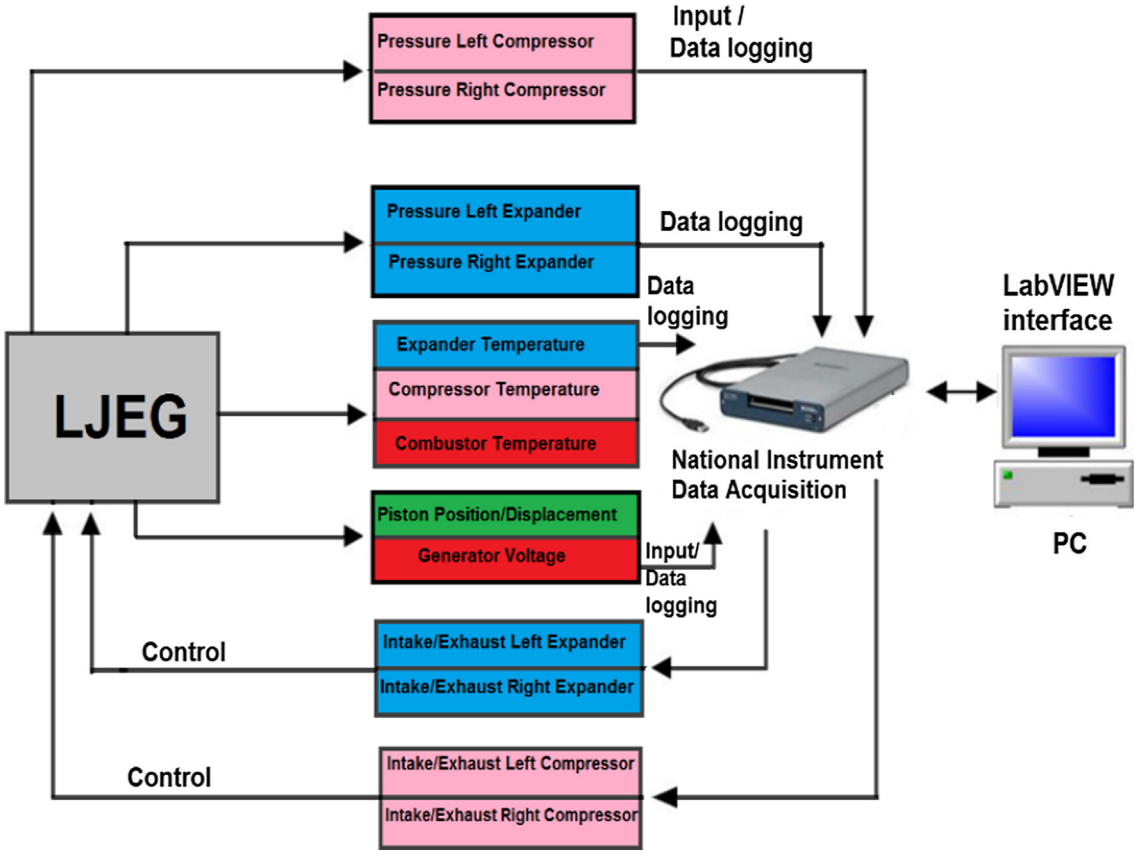

Fig. 4. Data acquisition and control system.

Table 2
Prototype specifications and input parameters for model validation.

	Parameters [Unit]	Value
System	Moving mass [kg]	27.5
Expander	Maximum stroke [mm]	120.0
	Effective bore [mm]	80.0
	Inlet pressure [bar]	2.7
	Inlet temperature [K]	473.0
	Valve diameter [mm]	32.5
	Valve lift [mm]	8.13
Compressor	Maximum stroke [mm]	120.0
	Effective bore [mm]	70.0
	Inlet pressure [bar]	1.0
	Outlet pressure [bar]	2.7
Linear generator	Load constant of the generator [N/m·s^{-1}]	0

the piston sliding velocity. The heat transfer between the in-cylinder gas and chamber walls of the expander is modelled accordingly [30]:

$$\dot{Q}_h = hA_e(T - T_w) \tag{17}$$

$$h = 130V^{-0.06}\left(\frac{p(t)}{10^5}\right)^{0.8} T^{-0.4}(\dot{x}_m + 1.4)^{0.8} \tag{18}$$

where $\dot{Q}_h$(J/s)is the heat flow rate; h (W/m^2·K) is the coefficient of heat transfer; A_e (m^2) is the area of the surface in contact with the gas in the expander; T_w (K) is the average surface temperature of the cylinder wall, V (m^3) is the instantaneous cylinder volume; $\dot{x}_m$(m/s) is the average piston speed. The mass flow rate through the valves, $\dot{m}$ (kg/s) is described by Eq. (19) [31].

$$\dot{m} = \begin{cases} \frac{C_d A_d p_u}{(RT_u)^{\frac{1}{2}}}\left(\frac{p_d}{p_u}\right)^{\frac{1}{\gamma}}\sqrt{\frac{2\gamma}{\gamma-1}\left[1-\left(\frac{p_d}{p_u}\right)^{\frac{(\gamma-1)}{\gamma}}\right]}, & p_d/p_u > [2/(\gamma+1)]^{\gamma/(\gamma-1)} \\ \frac{C_d A_d p_u}{(RT_u)^{1/2}}\gamma^{1/2}\left(\frac{2}{\gamma+1}\right)^{(\gamma+1)/2(\gamma-1)}, & p_d/p_u \le [2/(\gamma+1)]^{\gamma/(\gamma-1)} \end{cases} \tag{19}$$

where $\dot{m}$ (kg/s) is the mass flow rate through valve; C_d is the discharge coefficient; A_d (m^2) is the reference area of the flow; T_u (K) is the temperature of the inlet gas; p_u (Pa) is the pressure of the upstream of the flow restriction; p_d (Pa) represents the downstream air pressure; R (J/kg K) gas constant. A mass flowrate leakage of 2% is allowed in Eq. (19) for the compressor and expander in the model. Electrical current is drawn from the coils of the linear generator through the continuous back and forth movement of the mover. The load force of the electric machine is assumed to be proportional to the current generated according to electromagnetic theory and its direction is always opposite to the piston velocity [32], the resistance force from the generator is described as:

$$\vec{F_g} = -G\dot{x} \tag{20}$$

where G (N/(ms^{-1})) is the linear generator load constant, $\dot{x}$ (m/s) is the piston velocity. Eq. (8) represents the friction force model adopted in the dynamic and thermodynamic model.

3. Experimental procedure

Compressed air (working fluid) from an external compressed air tank is heated in the reactor during starting operation, before it flows from the reactor to the expander. The high energy fluid expands in the expander and drives the compressor. The compressed air from the compressor is piped into the reactor where its energy content is increased at constant pressure before it goes to the expander to continue the cycle. The external supply of the compressed air is shut off once the system compressor is in operation. The expander inlet valve opens when the expander piston is at its Operation Top Dead Centre (OTDC). The expander piston is driven by the compressed air and moves from its OTDC to its Operation Bottom Dead Centre (OBDC), i.e. from the left to the right for the left expander chamber and from right to left, for the right expander chamber, until the expansion process is completed (Fig. 1a). While the working fluid in the left expander is undergoing expansion, the expansion work powers the right compressor simultaneously. Similarly, an expansion process in the right expander powers the left compressor simultaneously. Fig. 4 shows the structure for data acquisition and control process. The data acquisition and control of the LJEG system are implemented using the National Instrument CompactRIO system, the program for monitoring and display of the real-time signals is developed in LabVIEW. The sensors are connected to I/O modules on the CompactRIO system for data collection. The collected data is temporarily stored in the CompactRIO memory and then streamed to the PC. The intake, exhaust and in-cylinder pressures of the expander and compressor were measured by pressure sensors; the piston position/displacement was measured by an incremental magnetic sensor and the intake and exhaust temperature of the reactor, the compressors, and the expanders were measured by temperature sensors. The measured piston displacement and the compressor output pressure were used as feedback signals to control the intake/exhaust valve timings.

The recorded experimental data; compressor pressure P_c, expander pressure P_e and piston displacement x, were used to calculate for the variables in Eq. (21). Where $F_e = P_e \times A_e$, $F_c = P_c \times A_c$, $A_e = \frac{\pi d_e^2}{4}$, $A_c = \frac{\pi d_c^2}{4}$, where F_f is the friction model in Eq. (8). The values for other input parameters during the experiment are listed in Table 2. See Fig. 5 and Table 3 for the details of the piston ring.

The following values were used for the constants in Eqs. (12) and (14); $a_1 = 21$, $a_2 = 0.9$, $z_1 = 183$, $z_2 = 80$, $f_s = 0.1$ and $f_d = 0.095$. Expander ring compression pressure is 0.02N/mm^2; compressor ring compression pressure is 0.0256 N/mm^2

$$F_f = F_e + F_c + F_g - m\frac{d^2x}{dt^2} \tag{21}$$

$$\frac{d^2x}{dt^2} = \frac{F_e + F_c + F_g + F_f}{m} \tag{22}$$

The observed test data friction force is obtained from the test data indirectly using the measured piston motion and in-cylinder pressure as represented in Eq. (21).

4. Results and discussions

4.1. Friction model results

Fig. 6 shows the comparison between the observed data and the simulated results of the proposed friction force model. The model result matches the trends of the observed test data. The observed errors seen in the plot are originated from noises in the in-cylinder pressure measurement.

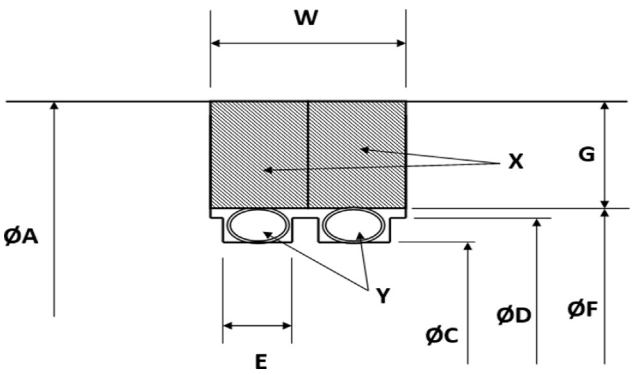

Fig. 5. Schematic of piston seal.

Table 3
Piston seal information.

X	2 Piston rings type	
Y	2 Canted springs	
	Expander (mm)	Compressor (mm)
Ring width W	10	8
Ring diameter A	80	70
C	67	57
D	70	60
E	3.2	3.2
F	68	61
G	6.0	4.5

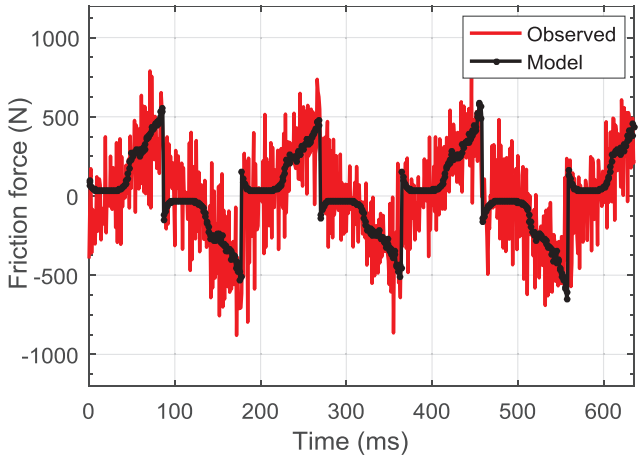

Fig. 6. The LJEG friction force profiles (from tests and the model).

To further validate the accuracy of the model, the measured and the calculated piston dynamics properties are compared. The acceleration profile of the LJEG is shown in Fig. 7, the line shown as the observed acceleration is calculated from the second derivative ($\frac{d^2x}{dt^2}$) of the measured piston displacement, while the line indicated as model acceleration is calculated from Eq. (22). All other variables in Eq. (22) are measured directly from the experiment, only the frictional force is calculated from Eq. (8).

A comparison is made between the proposed model and other reported models that could fit in the LJEG dry friction analysis scenario. The reported friction models are categorised into Cases 1–4 as presented in Table 4.

The required experimental data were imported to MATLAB and all models (including models in Cases 1–4) were implemented in MATLAB/Simulink environment. The parameters for Case 1–4 were optimised. Figs. 8, 9 and 10 show the accelerations, the velocities and the displacements generated from the models of Cases 1–4, the proposed model and the experiments of the LJEG.

Fig. 11 and Table 5 explain the operation modes of the LJEG. Fig. 12 demonstrates the piston velocity and trend of total friction force development across the LJEG. Point 1 indicates the start of expansion for the left expander; with the expander piston at OTDC position while the right compressor piston is at OBDC. Point 2 indicates inlet valve closure of the right compressor; therefore, technically compression in the right compressor starts at “2”, while point 3 marks the close of the left expander inlet valve. At point 4, the right compressor exhaust valve opens, point 5 marks the end of compression and the OTDC for the right compressor and OBDC for the left compressor. Compression continues from point “2” to point “5” although the compressor outlet valve opens at “4”. Processes between points 6–10 are the same as point 1 to point 5 for the right expander and left compressor. Fig. 13 shows the time history of piston velocity and friction force contribution due to dry contact friction of the piston ring and cylinder liner, while Fig. 14 shows the time history of compressor pressure and friction force contribution due to pressure loading.

Figs. 15 and 16 show total friction force with the piston velocity and the piston displacement respectively. It can be observed from Figs. 12, 15 and 16 that the friction force is closely related to the compression process in the LJEG. The friction force peaking range corresponds to the compression process in the LJEG (see Figs. 12 and 14). It implies that the friction during the compression phase is more significant when compared with friction during the expansion process and the friction tends to increase proportionally with the rise of the compression pressure.

At the start of expansion; point 1 (Figs. 12, 15 and 16), the friction force is higher than other times during expansion (points 1–3); this effect is because of the higher stiction due to piston sticking at OTDC/OBDC.

The friction force of the piston takes on a sharply rising trend between “point 3” and point 4” (See Figs. 12, 14, 15 and 16), which corresponds to the region of higher piston velocity. It implies that within the region of higher piston velocity and the compressor outlet valve opening “4”, the increase of the friction force is due to the increase in compressor pressure rather than the effect of piston velocity (see Eq. (13)).

It was observed that the compression process starts at point 2 and through points 4 to 5 (see Figs. 12, 15 and 16). Compressor outlet valve opens at “point 4” and closes at “point 5”; whilst the pressure between “point 4” and “point 5” is the same, the friction force is found to be increasing between the two points. The continuous increase in friction force at constant pressure (between “4” and “5”) can be attributed to a continuous decrease in piston velocity (see exponential part of Eq. (13)) between the points and increase in pressure of air cushion at the expander, due to early closing of the expander exhaust valve.

Shortly after the start of expansion (after “point 1”, see Fig. 16), the friction force is almost uniform until the start of compression (“point 2”), dry friction contributes more than 80% to the total friction before the start of compression. Between the start of (“point 2”) and the end (“point 5”) of compression, friction due to the pressure loading contributes over 85% of the total friction force. Generally, the total friction of the LJEG pistons increases continuously at the start of compression, attains the peak point at the end of compression. The total friction force changes its sign when the piston begins its reverse stroke after OTDC, and continues in the reverse direction and gradually reduces following the expansion process. Fig. 17 shows the frictional power for a complete cycle of the LJEG.

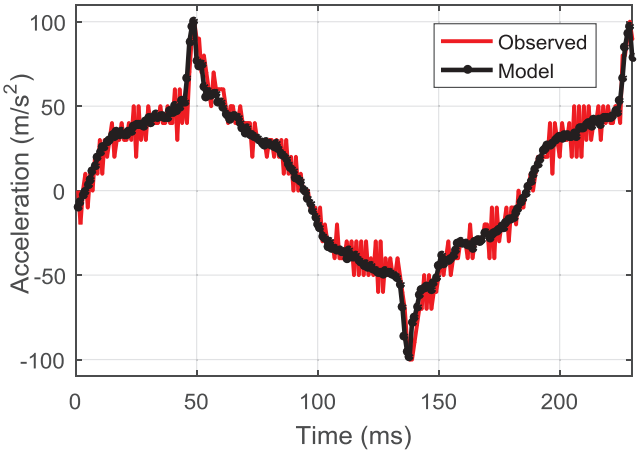

Fig. 7. Piston acceleration profile.

Table 4
Reported friction models applicable to LJEG operating on dry friction mechanism.

S/N	Description	Expression
Case 1 [20–22]	This model considers the friction force to be a constant throughout the entire stroke	Numerical constant (300^{**})
Case 2 [14–16]	This friction model describes friction force behaviour as a viscous force; it models the friction force as a force proportional to the sliding velocity while the direction of friction is opposite to sign of piston velocity	$F_{friction}(t) = -k\dot{x}(t)$ where k represents a proportionality constant and $\dot{x}$; the instantaneous sliding velocity. ($k = 250^{**}$)
Case 3 [17–19]	This friction model describes frictional force of having both static and viscous friction force components	$F_{friction}(t) = sign(\dot{x})[k_1 + k_2\ \lvert\dot{x}(t)\rvert]$ where $\dot{x}$; the instantaneous sliding velocity, k_2 is the viscous friction coefficient related to the instantaneous velocity, and k_1 is the Coulomb friction coefficient which is considered as a constant part of frictional force. ($k_1 = 230^{**}$ and $k_2 = 100^{**}$)
Case 4 [23]	The friction model consists of three friction components; viscous friction, Coulomb friction and friction force as a result of in-cylinder pressure loading	$F_{friction}(t) = C_f\dot{x} + f_d(T_r + \pi p D_p w_p)$ where C_f represents damping coefficient, f_d dynamic friction coefficient, T_r is the diametral force, p is the in-cylinder pressure, $w_p$is the width of piston ring and D_p is the piston diameter. ($C_f = 210^{**}$ and $f_d = 0.095^{**}$)

** Optimised parameters selected for simulation.

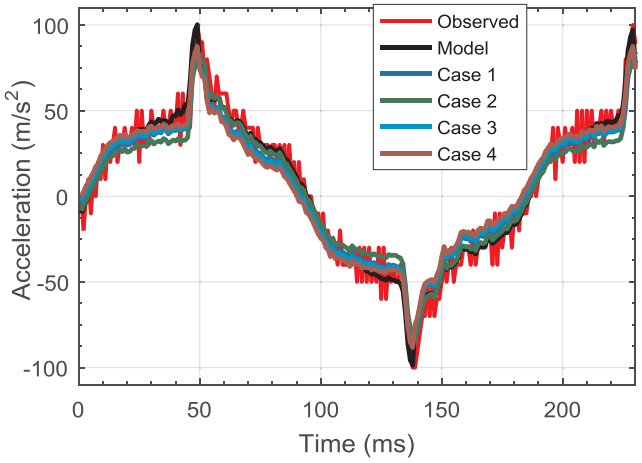

Fig. 8. Piston acceleration profile for different cases.

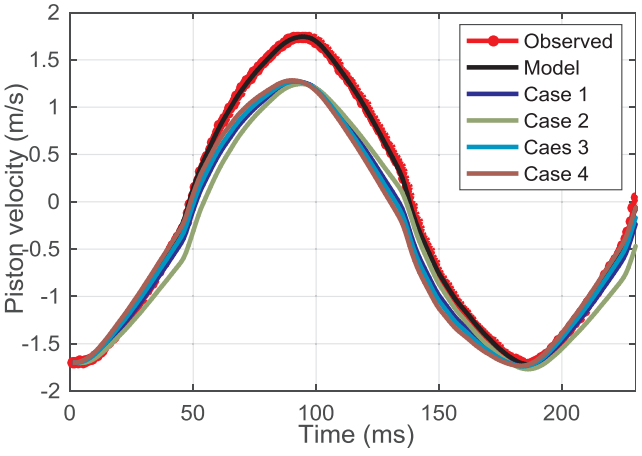

Fig. 9. Piston velocity profiles of different cases.

4.2. Dynamic and thermodynamic model results

A dynamic and thermodynamic model of the LJEG has been validated in the previous study [3] using a simplified friction model. The updated results after using the new friction model is presented here. The piston velocity, the displacement, and the velocity versus displacement profiles of both the improved model and the experiments at

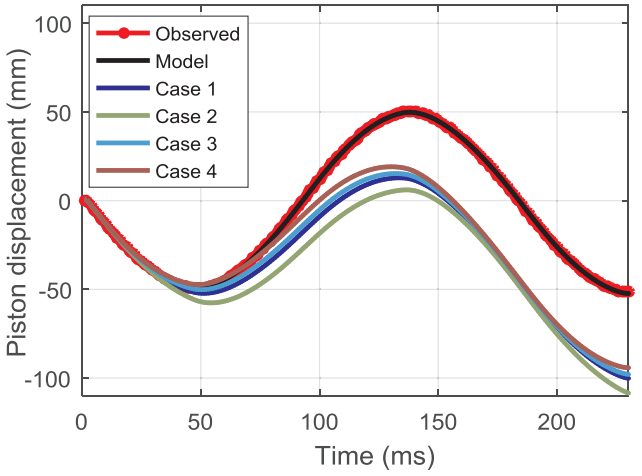

Fig. 10. Piston displacement profiles of different cases.

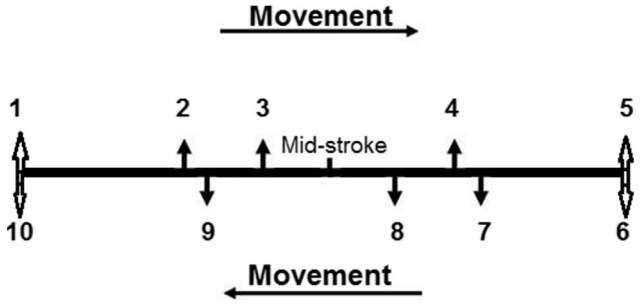

Fig. 11. Illustration of expander and compressor operation in the LJEG.

the same operating condition as Table 2 are presented in Figs. 18, 19 and 20 respectively. The piston dynamics predicted from the model shows similar trends with the experimental results, and the observed amplitudes are almost identical. The observed difference is acceptable due to the simplifications and the assumptions made when the authors linearize the model. The model is considered to be robust to evaluate the actual system performance of the LJEG prototype.

The coefficient of electric resistance force is the most influential parameter for the electricity generation efficiency in the LJEG [33]. It suggested that an efficiency of 80% can be achieved by increasing the coefficient of electric resistance force in the LJEG. Fig. 21 shows the mean friction power at different generator load conditions while

Table 5
Summary of expander and compressor operation in LJEG.

Point 1	OTDC for the left expander: left expander intake valve opens.
	OBDC for the right compressor: right compressor intake valve opens.
Point 2	Right compressor intake valve closes: start of compression.
Point 3	Left expander intake valve closes.
Point 4	Right compressor exhaust valve opens.
Point 5	OBDC for the left expander.
	OTDC for the right compressor: right compressor exhaust valve closes.
Point 6	OTDC for the right expander: right expander intake valve opens.
	OBDC for the left compressor: left compressor intake valve opens.
Point 7	Left compressor intake valve closes: start of compression.
Point 8	Right expander intake valve closes.
Point 9	Left compressor exhaust valve opens.
Point 10	OBDC for the right expander.
	OTDC for the left compressor: left compressor exhaust valve closes.

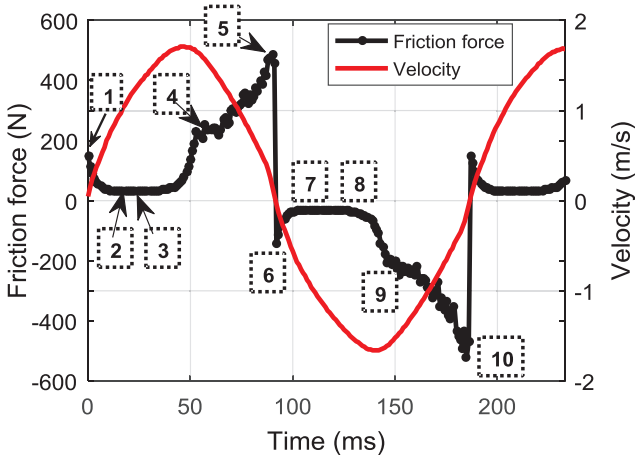

Fig. 12. Total friction force and piston velocity profile.

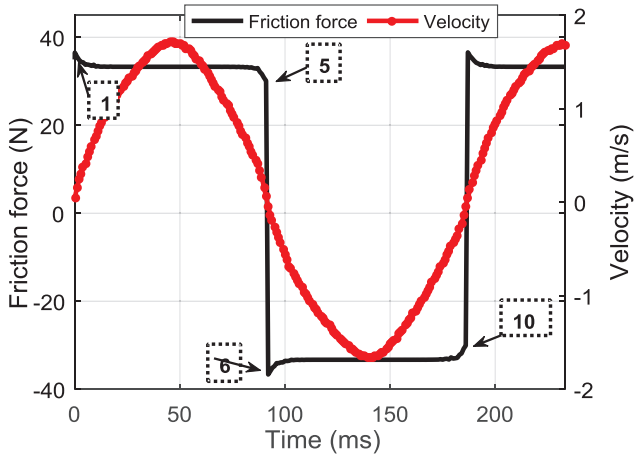

Fig. 13. Dry contact friction force and velocity profile.

keeping all other parameters of the LJEG constant. The operating condition is the same as Table 2 but with changes in operating pressure and temperature (shown in Table 6). It can be observed from Fig. 21 that the mean friction power of the LJEG varies inversely to the generator load when other parameters are kept constant. An increase in generator load means an increase in electromagnetic load resistance, which results to decreases in both piston amplitude and mean velocity. The relationship between generator load and friction power confirms that higher electric resistance force will result to lower friction force which improves the overall system efficiency.

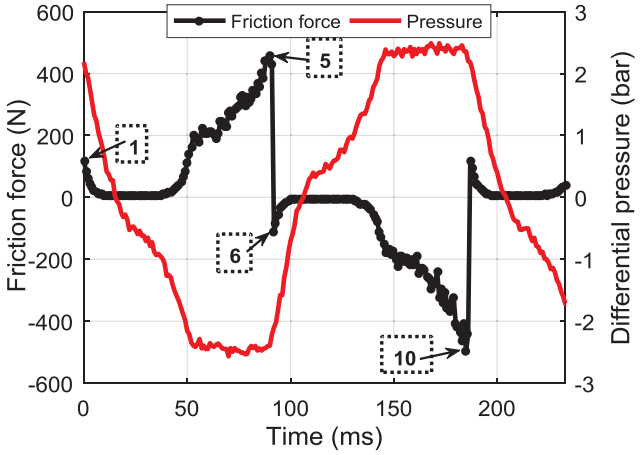

Fig. 14. Pressure friction force and compressor pressure profile.

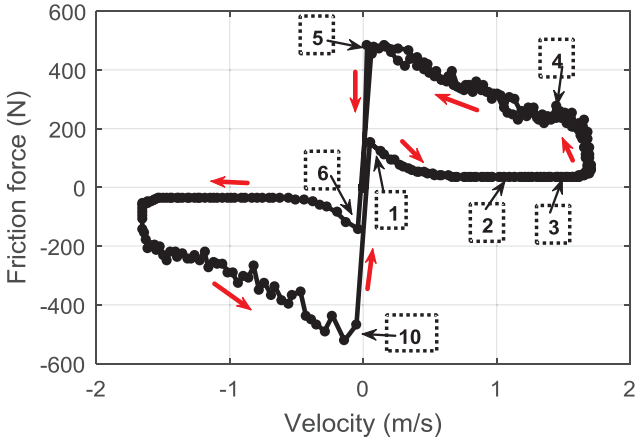

Fig. 15. Total friction force and piston velocity.

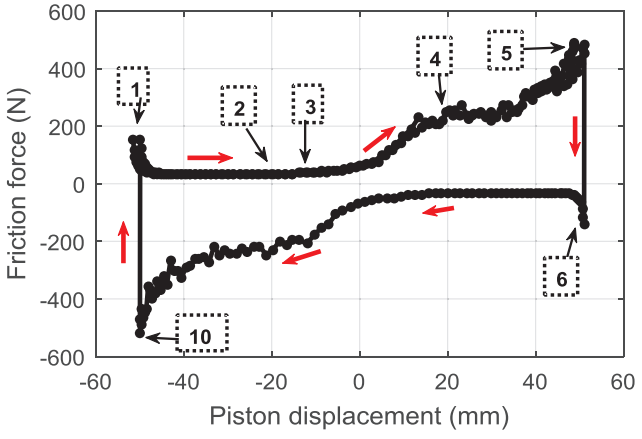

Fig. 16. Total friction force and piston displacement.

5. Conclusions

In this paper, a novel friction model of a Linear Joule Engine Generator (LJEG) is presented and the model validated with experimental data. The proposed friction model accounts for an only macroscopic sliding phenomenon. The major advantage of the proposed model is its simplicity and accuracy for numerical simulations. The main conclusions from this work are listed below:

The frictional force of the LJEG can be represented as a combination of a dry friction model from a mass-spring-damper system and a friction

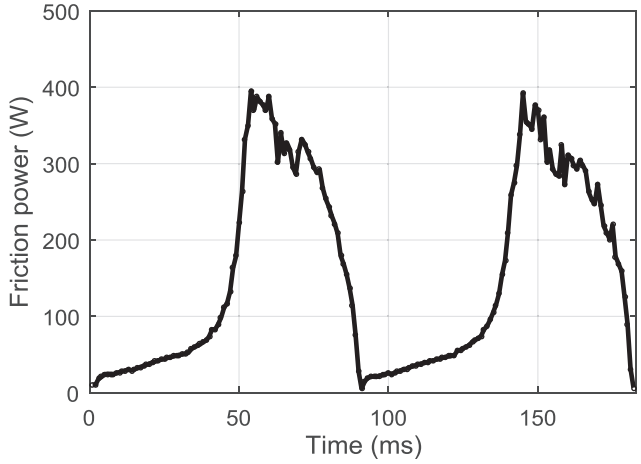

Fig. 17. Total frictional power loss for a complete cycle.

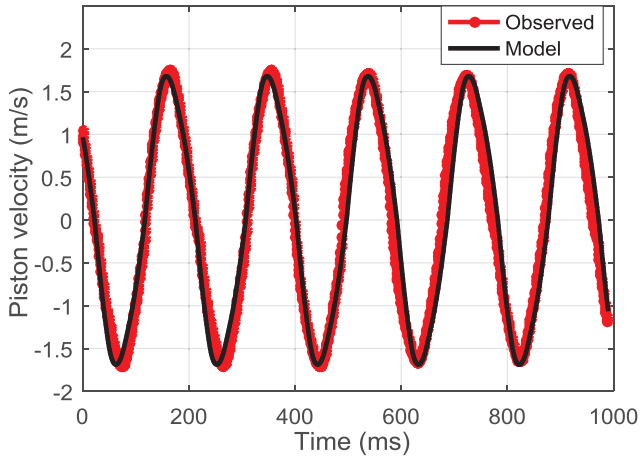

Fig. 18. Piston velocity profile.

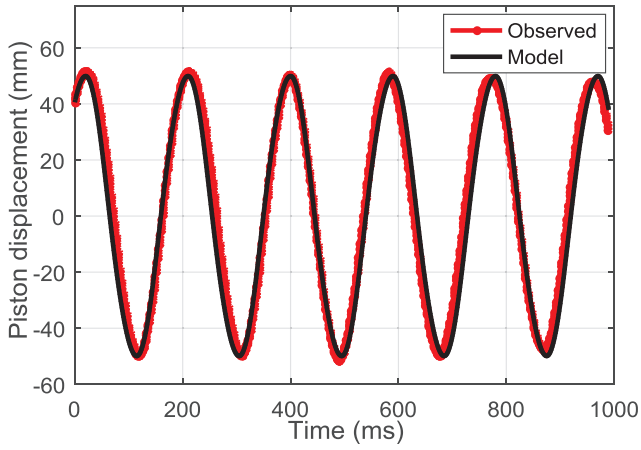

Fig. 19. Piston displacement profile.

force due to pressure of the working fluid. The mean friction force during the compression process is about 500% of the mean friction force during the expansion process. The pressure build-up in the Linear Joule Engine Generator compressor contributes a greater part of the friction force.

Apart from the surface characteristics of the piston ring and the cylinder liner interface, the system pressure, the piston velocity and the piston acceleration are the main parameters defining the friction characteristics of Linear Joule Engine Generator.

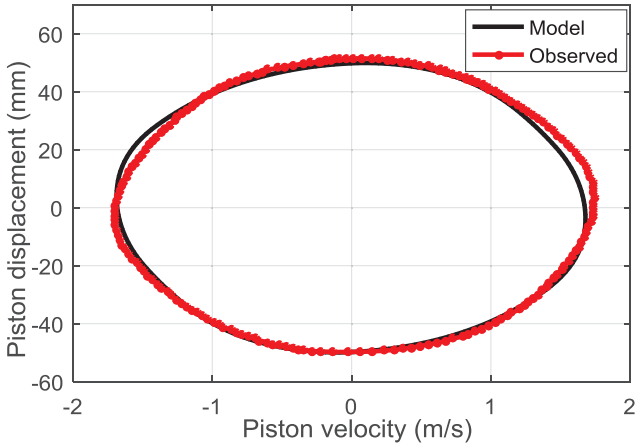

Fig. 20. Piston velocity vs. displacement.

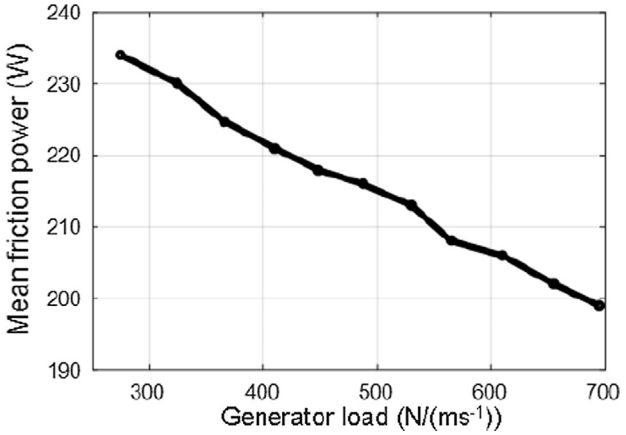

Fig. 21. Mean friction power at different generator load.

Table 6
Input parameters for the simulation.

	Parameters [Unit]	Value
Linear expander	Inlet pressure [bar]	7
	Inlet temperature [K]	1100
Linear compressor	Outlet pressure [bar]	7
	Inlet temperature [K]	300
	Outlet temperature [K]	473.0
Linear generator	Load [Nm/s]	Variable

The relationship between generator load and friction power shows that higher electric resistance force will result in lower friction which improves the overall system efficiency.

Acknowledgement

This work was funded by grants from Innovate UK (132757) and EPSRC (UK Engineering and Physical Sciences Research Council) (EP/R041970/1) both from the United Kingdom. Data supporting this publication is openly available under an 'Open Data Commons Open Database License'. Additional metadata are available at: http://dx.doi.org/10.17634/173043-2. Please contact Newcastle Research Data Service at rdm@ncl.ac.uk for access instructions.

References

[1] Mikalsen R, Roskilly AP. The free-piston reciprocating Joule Cycle engine: a new approach to efficient domestic CHP generation. Proceeding of ICAE2012 conference. 2012.

[2] Wu D, Roskilly AP. Design and parametric analysis of linear Joule-cycle engine with out-of-cylinder combustion. Energy Procedia 2014;61:1111–4.
[3] Jia B, Wu D, Smallbone A, Lawrence C, Roskilly AP. Design, modelling and validation of a linear Joule Engine generator designed for renewable energy sources. Energy Convers Manage 2018;165:25–34.
[4] Wang Y, Chen L, Jia B, Roskilly AP. Experimental study of the operation characteristics of an air-driven free-piston linear expander. Appl Energy 2017;195:93–9.
[5] Bell MA, Partridge T. Thermodynamic design of a reciprocating Joule cycle engine. Proc Inst Mech Eng, Part A: J Power Energy 2003;217(3):239–46.
[6] Moss RW, Roskilly AP, Nanda SK. Reciprocating Joule-cycle engine for domestic CHP systems. Appl Energy 2005;80(2):169–85.
[7] Creyx M, Delacourt E, Morin C, Desmet B, Peultier P. Energetic optimization of the performances of a hot air engine for micro-CHP systems working with a Joule or an Ericsson cycle. Energy 2013;49:229–39.
[8] Lontsi F, Hamandjoda O, Fozao K, Stouffs P, Nganhou J. Dynamic simulation of a small modified Joule cycle reciprocating Ericsson engine for micro-cogeneration systems. Energy 2013;63:309–16.
[9] Wu D, Jalal AS, Baker N. A coupled model of the Linear Joule Engine with embedded tubular permanent magnet linear alternator. Energy Procedia 2017;105:1986–91.
[10] Hou X, Zhang H, Yu F, Liu H, Yang F, Xu Y, et al. Free piston expander-linear generator used for organic Rankine cycle waste heat recovery system. Appl Energy 2017;208:1297–307.
[11] Hou X, Zhang H, Xu Y, Yu F, Zhao T, Tian Y, et al. External load resistance effect on the free piston expander-linear generator for organic Rankine cycle waste heat recovery system. Appl Energy 2018;212:1252–61.
[12] Cater MS, Bolander NW, Sadeghi F. Experimental investigation of surface modifications for piston-ring/cylinder-liner friction reduction. ASME 2008 internal combustion engine division spring technical conference, 2008, January. American Society of Mechanical Engineers; 2008. p. 355–65.
[13] Jia B, Mikalsen R, Smallbone A, Roskilly AP. A study and comparison of frictional losses in free-piston engine and crankshaft engines. Appl Therm Eng 2018;140:217–24.
[14] Tian CL, Feng HH, Zuo ZX. Oscillation characteristic of single free piston engine generator. Advanced materials research. Trans Tech Publications; 2012. p. 1873–8.
[15] Zhang C, Chen F, Li L, Xu Z, Liu L, Yang G, et al. A free-piston linear generator control strategy for improving output power. Energies 2018;11(1):135.
[16] Xu Y, Tong L, Zhang H, Hou X, Yang F, Yu F, et al. Experimental and simulation study of a free piston expander–linear generator for small-scale organic Rankine cycle. Energy 2018;161:776–91.
[17] Goldsborough SS, Van Blarigan P. A numerical study of a free piston IC engine operating on homogeneous charge compression ignition combustion (No. 1999-01-0619). SAE Technical Paper; 1999.
[18] Lee CP. Turbine-compound free-piston linear alternator engine. University of Michigan. PhD Dissertation; 2014.
[19] Gusev S, Ziviani D, Vierendeels J, De Paepe M. Variable volume ratio free-piston expander: prototyping and experimental campaign. Int J Refrig 2018.
[20] Atkinson CM, Petreanu S, Clark NN, Atkinson RJIMT, Nandkumar S, Famouri P. Numerical simulation of a two-stroke linear engine-alternator combination. SAE Technical Paper 1999-01-0921; 1999.
[21] Feng H, Song Y, Zuo Z, Shang J, Wang Y, Roskilly AP. Stable operation and electricity generating characteristics of a single-cylinder free piston engine linear generator: simulation and experiments. Energies 2015;8(2):765–85.
[22] Mikalsen R, Roskilly AP. The design and simulation of a two-stroke free-piston compression ignition engine for electrical power generation. Appl Therm Eng 2008;28(5–6):589–600.
[23] Yuan C, Xu J, He Y. Parametric study on the starting of a free-piston engine alternator. Int J Engine Res 2018;19(4):411–22.
[24] Wakuri Y, Soejima M, Ejima Y, Hamatake T, Kitahara T. Studies on friction characteristics of reciprocating engines. SAE Trans 1995:1463–77.
[25] Jia B, Smallbone A, Feng H, Tian G, Zuo Z, Roskilly AP. A fast response free-piston engine generator numerical model for control applications. Appl Energy 2016;162:321–9.
[26] Jia B, Zuo Z, Smallbone A, Feng H, Roskilly AP. A decoupled design parameter analysis for free-piston engine generators. Energies 2017;10(4):486.
[27] Wiercigroch M, Sin VWT, Liew ZFK. Non-reversible dry friction oscillator: design and measurements. Proc Inst Mech Eng, Part C: J Mech Eng Sci 1999;213(5):527–34.
[28] Stefański A, Wojewoda J, Wiercigroch M, Kapitaniak T. Chaos caused by non-reversible dry friction. Chaos Soli Fractals 2003;16(5):661–4.
[29] Powell J, Wiercigroch M. Influence of non-reversible Coulomb characteristics on the response of a harmonically excited linear oscillator. Mach Vib 1992;1(2):94–104.
[30] Hohenberg GF. Advanced approaches for heat transfer calculations (No. 790825). SAE Technical Paper 1979.
[31] Heywood JB. Internal combustion engine fundamentals. New York: McGraw-Hill; 1988.
[32] Polinder H, Slootweg JG, Hoeijmakers MJ, Compter JC. Modeling of a linear PM machine including magnetic saturation and end effects: maximum force-to-current ratio. IEEE Trans Ind Appl 2003;39(6):1681–8.
[33] Jia B, Wu D, Smallbone A, Ngwaka UC, Roskilly AP. Dynamic and thermodynamic characteristics of a Linear Joule Engine Generator with different operating conditions. Energy Convers Manage 2018;173:375–82.